Improving Boundary Element Methods for Parasitic Extraction*

Shu Yan
Dept. of Electrical Engineering
Texas A&M University
College Station, TX 77843
shu@ee.tamu.edu

Jianguo Liu
Dept. of Mathematics
University of North Texas
Denton, TX 75203
jgliu@unt.edu

Weiping Shi
Dept. of Electrical Engineering
Texas A&M University
College Station, TX 77843
wshi@ee.tamu.edu

Abstract - We improve the accuracy and speed of boundary element method (BEM) or multipole accelerated BEM for interconnect parasitic extraction. Three techniques are presented and applied to capacitance extraction: selective coefficient enhancement, variable order multipole and multigrid. Experimental results show that the techniques are effective for extracting parasitics between all pairs of conductors, or between selected pairs of conductors.

I. Introduction

Many 3D parasitic extraction algorithms are based on the Boundary Element Method (BEM), and accelerated with the Fast Multipole Method (FMM) [8], such as FastCap [12], FastHenry [9], hierarchical refinement [15], multi-scale [16], and others [3, 17]. Algorithms based on BEM but not FMM include the pre-corrected FFT algorithm [13], and the singular value decomposition algorithm [10].

The capacitance of an m-conductor geometry is summarized by an $m \times m$ capacitance matrix $\mathbf{C}$. To determine the j-th column of the capacitance matrix, we compute the surface charges on each conductor produced by raising conductor j to unit potential while grounding the other conductors. Then C_{ij} is numerically equal to the charge on conductor i. This procedure is repeated m times to compute all columns of $\mathbf{C}$.

In the BEM, each of the m potential problems can be solved using an equivalent free-space formulation where the conductor-dielectric interface is replaced by a charge layer of density σ. The charge layer satisfies the integral equation

$$\psi(x) = \int_{surfaces} \sigma(x') \frac{1}{4\pi\epsilon_0 \|x - x'\|} da', \qquad (1)$$

where $\psi(x)$ is the known conductor surface potential, da' is the incremental conductor surface area, x, $x' \in \Re^3$, $x' \in da'$, and $\|x - x'\|$ is the Euclidean distance between x and x'.

*This research was supported by NSF grants CCR-0098329, CCR-0113668, EIA-0223785, and ATP grant 512-0266-2001.

Galerkin scheme is often used to numerically solve (1) for σ. In this approach, the conductor surfaces are divided into n small panels, and on each panel A_i, a charge q_i is assumed uniformly distributed. Then for each panel A_i, an equation is written which relates the known potential on A_i, denoted by v_i, to the sum of the contribution of potential from charges on all n panels $A_1, A_2, \ldots, A_n$. The result is a dense linear system

$$\mathbf{Pq} = \mathbf{v}, \qquad (2)$$

where $\mathbf{q} \in \Re^n$ is the vector of panel charges, $\mathbf{v} \in \Re^n$ is the vector of known panel potentials, and $\mathbf{P} \in \Re^{n \times n}$ is the potential coefficient matrix. Each entry of $\mathbf{P}$ is defined as

$$p_{kl} = \frac{1}{area(A_k)} \int_{A_k} \frac{1}{area(A_l)} \int_{A_l} \frac{1}{4\pi\epsilon_0 \|x_k - x_l\|} da_l da_k, \qquad (3)$$

for panels A_k and A_l. The integration in (3) is computed by numerical methods. The linear system (2) has to be solved to compute panel charges, and the capacitances are derived by summing the panel charges. Because $\mathbf{P}$ is dense and large, iterative methods, such as GMRES [14], are used for solving the equation.

The BEM involves approximation errors from the following sources.

- Panel discretization, due to the assumption of uniform charge distribution on each panel.
- Approximation of $\mathbf{P}$, due to the numerical integration of (3) and truncation of multipole expansion.
- Iterative solution for $\mathbf{Pq} = \mathbf{v}$.

Among the three errors, the first type is dominant. Although fine discretization reduces error, it also results in large linear systems and unacceptable computation time. The adaptive refinement scheme [15, 17] and high order basis functions [5] are popular ways used to reduce the first type of error. In [1], the adaptive meshing idea of constructing an optimal mesh based on a coarse initial discretization was studied. However, no implementation and running time were reported. In this paper, we propose a multigrid scheme [4] that reduces the number of iterations for solving a large dimension linear system by

using a good initial solution based on coarse discretization. This helps to preserve high accuracy while reduce the computation cost greatly.

The error of the second type is the main focus of this paper, and two techniques are proposed: the variable order multipole scheme and the selective enhancement scheme. In [7], the hierarchical algorithm of Barnes and Hut [2] was modified to allow high order expansion for nodes high in the tree, and low order expansion for nodes low in the tree. Their variable order expansion method [7] is static and does not change with the charge distribution as the GMRES algorithm progresses. The adaptive multipole order method using an error indicator is studied in [1]. However, no simulation results were given to compare the overhead and overall efficiency.

For crosstalk and signal integrity analysis, it is desirable to compute the parasitic between some conductors with high accuracy. In this paper, we study how to do this without significantly increasing the overall computation time.

To reduce the third type of error, the number of iterations is usually increased. We apply the multigrid method [4] to reduce the number of iterations. The multigrid method is also helpful to reduce the first type of error as discussed above.

The methods proposed in this paper can be applied to inductance extraction as well. Using the mesh formulation of [11], the conductor surfaces can be partitioned into a hierarchy of meshes. The unknowns are mesh currents, similar to charge for the capacitance extraction problem. The linear system to be solved is $\mathbf{M}(\mathbf{R}+\mathbf{j}\omega\mathbf{L})\mathbf{M^T}=\mathbf{V}$, see [11]. Therefore, the same ideas can be applied.

In this paper, the implementations of all our new schemes are based on the hierarchical algorithm [15]. This is because the hierarchical algorithm is shown to be much faster than FastCap [12]. This is also because the traditional FMM algorithms [8, 12] are too expensive to modify for different coefficients, different expansion orders, and are kernel dependent.

In Section II, we first present the technique of sensitivity analysis for linear systems to study the accuracy of entries of $\mathbf{C}$ with respect to the accuracy of $\mathbf{P}$. Then, based on this technique, we propose the selective enhancement scheme and experiments are included as well. In Section III, we propose a new error analysis for FMM that illustrates the relationship between error and charge distribution. Following the analysis, we present the variable order multipole scheme and give experimental results. In Section IV, we apply multigrid method to capacitance extraction. Finally in Section V, we conclude our findings.

II. Selective Enhancement

A. Coefficient Matrix Approximation

Now we present a theory on the accuracy of selected entries of $\mathbf{C}$. Due to the second type of error, instead of $\mathbf{Pq}=\mathbf{v}$, the linear system we actually solve is

$$\bar{\mathbf{P}}\bar{\mathbf{q}}=\mathbf{v}, \tag{4}$$

where $\bar{\mathbf{P}}$ is an approximation of $\mathbf{P}$ and $\bar{\mathbf{q}}$ is the corresponding solution. As a result, the capacitance matrix obtained is an approximation $\bar{\mathbf{C}}$ instead of $\mathbf{C}$.

Assume there are k_i panels on the i-th conductor, and the panels are numbered in ascending order from the first conductor to the m-th conductor. To calculate the j-th column of $\bar{\mathbf{C}}$, we first solve (4) with $\mathbf{v}=\mathbf{v}^{(j)}=[0,\ldots,0,1,\ldots,1,0,\ldots,0]^T$, where the first $k_1+\cdots+k_{j-1}$ entries of $\mathbf{v}^{(j)}$ are 0, followed by k_j 1's and $n-(k_1+\cdots+k_j)$ 0's. Then for $i=1,2,\ldots,m$,

$$\bar{C}_{ij}=\sum_{l=k_1+\cdots+k_{i-1}+1}^{k_1+\cdots+k_i}\bar{\mathbf{q}}_l^{(j)}, \tag{5}$$

where $\bar{\mathbf{q}}^{(j)}$ is the solution of (4) corresponding to the right-hand side $\mathbf{v}=\mathbf{v}^{(j)}$. Similarly, if $\mathbf{q}^{(j)}$ denotes the solution of (2) corresponding to the right-hand side $\mathbf{v}=\mathbf{v}^{(j)}$, then entry C_{ij} of the capacitance matrix is given by

$$C_{ij}=\sum_{l=k_1+\cdots+k_{i-1}+1}^{k_1+\cdots+k_i}\mathbf{q}_l^{(j)}. \tag{6}$$

Let $\mathbf{r}^{(l)}$ denote the l-th column of $\mathbf{P}^{-1}$, then we have the following result.

Lemma 1 *For every $j=1,2,\ldots,m$, vector $\mathbf{q}^{(j)}$ and the columns of $\mathbf{P}^{-1}$ satisfy the equation*

$$\mathbf{q}^{(j)}=\sum_{l=k_1+\cdots+k_{j-1}+1}^{k_1+\cdots+k_j}\mathbf{r}^{(l)}.$$

Proof. It follows from the definition of $\mathbf{r}^{(l)}$ that $\mathbf{Pr}^{(l)}=\mathbf{e}^{(l)}$ where $\mathbf{e}^{(l)}$ denotes the l-th column of the identity matrix. Therefore

$$\begin{aligned}\mathbf{P}\cdot\Big(\sum_{l=k_1+\cdots+k_{j-1}+1}^{k_1+\cdots+k_j}\mathbf{r}^{(l)}\Big) &= \sum_{l=k_1+\cdots+k_{j-1}+1}^{k_1+\cdots+k_j}\mathbf{Pr}^{(l)}\\ &= \sum_{l=k_1+\cdots+k_{j-1}+1}^{k_1+\cdots+k_j}\mathbf{e}^{(l)}\\ &= \mathbf{v}^{(j)}.\end{aligned}$$

On the other hand, $\mathbf{P}q^{(j)}=\mathbf{v}^{(j)}$, therefore

$$\mathbf{q}^{(j)}=\sum_{l=k_1+\cdots+k_{j-1}+1}^{k_1+\cdots+k_j}\mathbf{r}^{(l)}.$$

□

Let $\mathbf{E}=\bar{\mathbf{P}}-\mathbf{P}$ be the error matrix. Then the following Lemma tells the relationship between the error of $\bar{C}_{ij}$ and $\mathbf{E}$.

Lemma 2 *Let $\bar{C}_{ij}$ and C_{ij} be given by (5) and (6) respectively, then $C_{ij} - \bar{C}_{ij} = (\mathbf{q}^{(i)})^T \mathbf{E} \bar{\mathbf{q}}^{(j)}$.*

Proof. From $\bar{\mathbf{P}}\bar{\mathbf{q}}^{(j)} = \mathbf{v}^{(j)}$ and $\mathbf{P}\mathbf{q}^{(j)} = \mathbf{v}^{(j)}$, we have $\mathbf{P}^{-1}\bar{\mathbf{P}}\bar{\mathbf{q}}^{(j)} = \mathbf{P}^{-1}\mathbf{v}^{(j)} = \mathbf{q}^{(j)}$. In other words, $\mathbf{P}^{-1}(\mathbf{P} + \mathbf{E})\bar{\mathbf{q}}^{(j)} = \mathbf{q}^{(j)}$. Hence $\mathbf{q}^{(j)} - \bar{\mathbf{q}}^{(j)} = \mathbf{P}^{-1}\mathbf{E}\bar{\mathbf{q}}^{(j)}$, which implies $q_l^{(j)} - \bar{q}_l^{(j)} = (\mathbf{P}^{-1}\mathbf{E}\mathbf{q}^{(j)})_l = (\mathbf{r}^{(l)})^T \mathbf{E}\mathbf{q}^{(j)}$, for any $j = 1, 2, \ldots, m$ and $l = 1, 2, \ldots, n$. The last equality holds because the matrix $\mathbf{P}$ is symmetric. Now using Lemma 1, formulas (5), (6), we have

$$\begin{aligned} C_{ij} - \bar{C}_{ij} &= \sum_{l=k_1+\cdots+k_{i-1}+1}^{k_1+\cdots+k_i} (q_l^{(j)} - \bar{q}_l^{(j)}) \\ &= \sum_{l=k_1+\cdots+k_{i-1}+1}^{k_1+\cdots+k_i} (\mathbf{r}^{(l)})^T \mathbf{E}\mathbf{q}^{(j)} \\ &= (\mathbf{q}^{(i)})^T \mathbf{E}\bar{\mathbf{q}}^{(j)}. \end{aligned}$$

□

Lemma 3 *Let $\mathbf{d} = \bar{\mathbf{q}} - \mathbf{q}$, $Cond(\mathbf{P})$ be the condition number of $\mathbf{P}$, and assume $\|\mathbf{E}\|/\|\mathbf{P}\| \leq 1/Cond(\mathbf{P})$. Then*

$$\mathbf{d} = -(\mathbf{I} + \mathbf{P^{-1}E})^{-1}\mathbf{P^{-1}Eq}.$$

Proof. Since $\mathbf{v} = \mathbf{P}\mathbf{q}$ and $\mathbf{v} = \bar{\mathbf{P}}\bar{\mathbf{q}} = (\mathbf{P} + \mathbf{E})(\mathbf{q} + \mathbf{d})$, we have $(\mathbf{P} + \mathbf{E})\mathbf{d} = -\mathbf{E}\mathbf{q}$. Therefore

$$\mathbf{d} = -(\mathbf{P} + \mathbf{E})^{-1}\mathbf{E}\mathbf{q} = -(\mathbf{I} + \mathbf{P^{-1}E})^{-1}\mathbf{P^{-1}Eq},$$

where $(\mathbf{I}+\mathbf{P^{-1}E})^{-1}$ exists because of the assumption. □

The condition $\|\mathbf{E}\|/\|\mathbf{P}\| \leq 1/Cond(\mathbf{P})$ is usually satisfied in practice. It simply says that the relative error of $\bar{\mathbf{P}}$ is small in comparison with $1/Cond(\mathbf{P})$.

Theorem 1 *Under the notations and assumptions of previous Lemmas, we have the following error representation*

$$C_{ij} - \bar{C}_{ij} = (\mathbf{q}^{(i)})^T \mathbf{E}\mathbf{q}^{(j)} - O(\|\mathbf{E}\|^2).$$

Proof. From Lemma 2 and Lemma 3,

$$\begin{aligned} & C_{ij} - \bar{C}_{ij} \\ = \; & (\mathbf{q}^{(i)})^T \mathbf{E}\bar{\mathbf{q}}^{(j)} \\ = \; & (\mathbf{q}^{(i)})^T \mathbf{E}\mathbf{q}^{(j)} - (\mathbf{q}^{(i)})^T \mathbf{E}\,(\mathbf{I} + \mathbf{P^{-1}E})^{-1}\mathbf{P^{-1}Eq}^{(j)} \\ = \; & (\mathbf{q}^{(i)})^T \mathbf{E}\mathbf{q}^{(j)} - O(\|\mathbf{E}\|^2). \end{aligned}$$

□

Corollary 1 *Let e_{kl} be any entry of $\mathbf{E}$, then*

$$\begin{aligned} & |C_{ij} - \bar{C}_{ij}| \\ \leq \; & |(\mathbf{q^{(i)}})^{\mathbf{T}}| \cdot |\mathbf{E}| \cdot |\mathbf{q^{(j)}}| + \mathbf{O}(\|\mathbf{E}\|^{\mathbf{2}}) \\ = \; & \sum_{k=1}^{n}\sum_{l=1}^{n} |q_k^{(i)}| \cdot |e_{kl}| \cdot |q_l^{(j)}| + O(\|\mathbf{E}\|^2) \\ = \; & \sum_{k=1}^{n}\sum_{l=1}^{n} (|q_k^{(i)}| \cdot |p_{kl}| \cdot |q_l^{(j)}|) \cdot \left|\frac{e_{kl}}{p_{kl}}\right| + O(\|\mathbf{E}\|^2). \end{aligned}$$

Proof. Follows immediately from Theorem 1. □

The relative errors $\left|\frac{e_{kl}}{p_{kl}}\right|$ for all pairs of k, l are usually of the same magnitude, depending on how the coefficients are computed. Corollary 1 says that the relative error is magnified by a factor $|q_k^{(i)}| \cdot |p_{kl}| \cdot |q_l^{(j)}|$. Therefore for those $\bar{p}_{kl}$ with large corresponding factor $|q_k^{(i)}| \cdot |p_{kl}| \cdot |q_l^{(j)}|$, we should compute $\bar{p}_{kl}$ with high accuracy. This helps to reduce the error for $|C_{ij} - \bar{C}_{ij}|$.

B. Application

In circuit simulation, the aggressor net and the victim net are often known in advance. Therefore we need to compute the coupling capacitance between the aggressor and the victim with high accuracy. For this situation, we have the following 2-phase scheme based on the above theory. In the first phase, the capacitance matrix is computed with the coefficient matrix of ordinary accuracy. In the second phase, potential coefficients are selectively refined according to charges computed in the first phase. The selected coupling capacitance is then recalculated.

Selective Enhancement Scheme
Input: Conductors, integers i, j and threshold θ.
Output: Capacitance matrix $\mathbf{C}$, where C_{ij} is computed at high accuracy.

Phase I: Initial computation.
1: Calculate $\mathbf{P}$ with ordinary accuracy.
2: For each conductor l, solve $\mathbf{P}\mathbf{q}^{(l)} = \mathbf{v}^{(l)}$.
3: Compute matrix $\mathbf{C}$.

Phase II: Selective enhancement.
4: For each entry p_{kl} of $\mathbf{P}$, if $|q_k^{(i)} \cdot p_{kl} \cdot q_l^{(j)}| \geq \theta$, recalculate p_{kl} using a more accurate method, and let the new coefficient matrix be $\mathbf{P'}$.
5: Solve equation $\mathbf{P'}\mathbf{q}^{(i)} = \mathbf{v}^{(i)}$ using the solution obtained in step 2 as the initial value.
6: Compute C_{ij} using $\mathbf{q}^{(i)}$.

In the algorithm, i and j denote the capacitance entry C_{ij} that needs to be computed to high accuracy. Input variable threshold θ is a user supplied value that affects the final accuracy for C_{ij}.

The implemented algorithm is executed on a SUN UltraSPARC Enterprise 4000, and tested for the 8 conductor example shown in Figure 1. Note that in step 4, the naive way to check all entries p_{kl} of $\mathbf{P}$ takes $O(n^2)$ time. However, since our algorithm stores matrix $\mathbf{P}$ in a data structure of size $O(n)$ [15], step 4 takes only $O(n)$ time.

Table I gives the experimental results, where the traditional method is either "no enhancement", meaning that all coefficients are computed at ordinary accuracy, or "full enhancement", meaning that all coefficients are computed

TABLE I
Experimental result for selective capacitance enhancement.

Capacitance		C_{00}	C_{01}	C_{10}	C_{11}	C_{12}	C_{21}	C_{22}	C_{23}	C_{32}	C_{33}
No Enhancement	Error (%)	2.62	3.94	3.99	3.61	4.56	4.41	3.53	4.21	4.15	3.57
	Time (sec)	59.18									
Selective Enhancement	Error (%)	0.88	0.79	0.77	0.61	0.95	0.89	0.92	0.54	0.62	0.94
	Time (sec)	64.8	64.6	66.2	67.6	65.7	65.8	66.8	65.9	65.5	66.9
	Time Increase (%)	9.5	9.2	11.9	14.3	11.0	11.2	12.9	11.4	10.7	13.1
Full Enhancement	Error (%)	0									
	Time (sec)	83.25									
	Time Increase (%)	41.1									

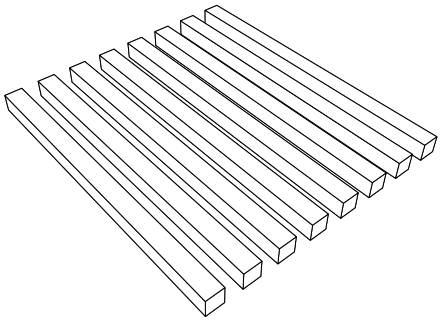

Fig. 1. The 8 conductor example.

at high accuracy. The high accuracy method uses 3×3 Gaussian quadrature, while the ordinary accuracy method uses the single point. The conductors are labeled from 0 at one side to 7 at the other side. Only self capacitance C_{ii} or coupling capacitance C_{ij} between adjacent conductors are significant enough to be considered. The error of a capacitance entry $\bar{C}_{ij}$ is defined as $|\bar{C}_{ij} - C_{ij}|/|C_{ij}|$, where C_{ij} is the capacitance computed by full enhancement method. That is why the full enhancement method has no error in the table. The "time increase" field is compared with the "no enhancement" method. Our GMRES reduces the two-norm residual to 1% from the initial residual.

The "no enhancement" method gives a less accurate capacitance matrix, while the "full enhancement" method consumes longer running time, compared with our selective enhancement scheme. Our method is suitable for applications where only a few entries of $\mathbf{C}$ need to be computed accurately. If we want to compute all entries of $\mathbf{C}$ accurately, then the full enhancement method is still faster.

III. Variable Order Multipole

A. Multipole Approximation

In the FMM method, the potential due to a set of charges located within a sphere can be approximated by a multipole series. However, the traditional error estimation of FMM [8] is expressed as a function of the radius of the sphere and the distance to the observation point. The error estimation is not expressed as a function of the location and amount of charge. In the following, we give an error estimation that takes into account the locations and values of charges.

For simplicity, let us consider the hierarchical refinement algorithm of [15]. The hierarchical refinement algorithm can be viewed as the 0-th order FMM, and is much easier to describe than the general FMM [8].

Theorem 2 *Assume we partition a panel A_k into two small panels A_1 and A_2 of equal shape and size. Let the radius of the smallest sphere that contains A_k be r_s. Consider panel A_l of distance r from the center of the sphere, for some $r > r_s$. Then the error of potential at A_l due to using A_k with charge $(q_1 + q_2)$ to approximate A_1 and A_2 with charges q_1 and q_2 respectively, is about*

$$\frac{|q_2 - q_1|}{2} \cdot \frac{r_s}{r} \cdot p_{kl}.$$

where p_{kl} is define in (3).

Proof. The potential at $x \in A_l$ due to the charge on panels A_1 and A_2, with uniform charge densities $\sigma_1 = q_1/area(A_1)$ and $\sigma_2 = q_2/area(A_2)$ is

$$\int_{x' \in A_1} \frac{\sigma_1}{4\pi\epsilon_0 \|x' - x\|} da' + \int_{x' \in A_2} \frac{\sigma_2}{4\pi\epsilon_0 \|x' - x\|} da'. \quad (7)$$

If we treat A_1 and A_2 as a single panel A with uniform charge density $(\sigma_1 + \sigma_2)/2$, then the potential at x will be

$$\int_{x' \in A} \frac{\sigma_1 + \sigma_2}{2} \frac{1}{4\pi\epsilon_0 \|x' - x\|} da'. \quad (8)$$

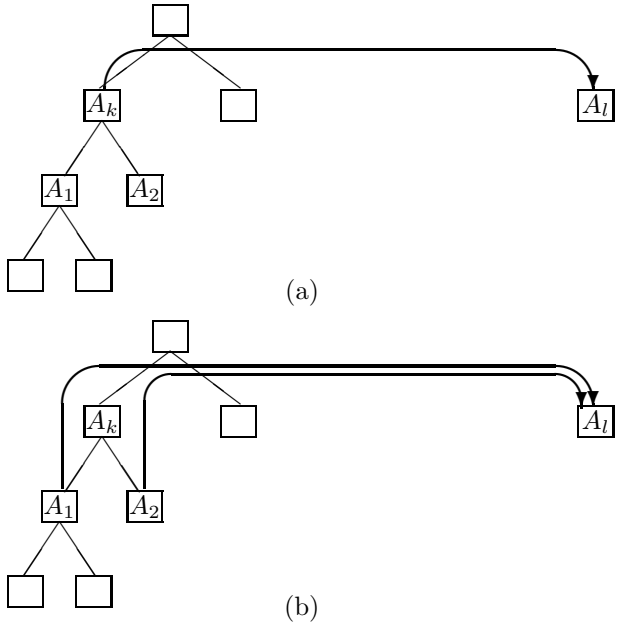

Fig. 2. In (a), assume $|q_2 - q_1| \cdot p_{kl}$ is less than a user supplied error bound. Therefore A_k interacts with A_l. In (b) assume otherwise. A_k passes the interaction down to A_1 and A_2.

Assume without loss of generality $\sigma_2 \geq \sigma_1$, then the difference between (7) and (8) is

$$\begin{aligned} & \frac{\sigma_2 - \sigma_1}{2} \frac{1}{4\pi\epsilon_0} \left(\int_{A_1} \frac{1}{\|x' - x\|} da' - \int_{A_2} \frac{1}{\|x' - x\|} da' \right) \\ \leq & \frac{\sigma_2 - \sigma_1}{2} \frac{1}{4\pi\epsilon_0} \int_{A_1} \left(\frac{1}{\|x' - x\|} - \frac{1}{\|x' - x\| + r_s} \right) da' \\ \leq & \frac{\sigma_2 - \sigma_1}{2} \frac{r_s}{r} \int_{A_1} \frac{1}{4\pi\epsilon_0 \|x' - x\|} da' \\ \approx & \frac{q_2 - q_1}{2} \cdot \frac{r_s}{r} \cdot p_{kl}. \end{aligned}$$

□

The ratio r_s/r decreases as r increases, which is fully exploited in the FMM. Now, we exploit the other factor $q_2 - q_1$, which has not been exploited before.

Previous study has illustrated the correlation between the error of potential and the error of charge distribution, see [1]. From this correlation, we expect to see a reduction of error in charge distribution if we reduce the error in potential. Our variable order multipole idea is thus derived from Theorem 2 and illustrated in Figure 2. On the left side of Figure 2, there is a hierarchy of panel discretization, where panel A_k is discretized as A_1 and A_2. For more information on the hierarchy algorithm, see [15]. In Figure 2(a), assume $|q_2 - q_1| \cdot p_{kl} \leq \theta$, where θ is a user supplied threshold. Therefore the error given in Theorem 2 is small, and A_1 and A_2 are treated as one panel A_k when interacting with A_l. In Figure 2(b), assume $|q_2 - q_1| \cdot p_{kl} > \theta$. Therefore A_1 and A_2 will interact with A_l directly. The interaction in Figure 2(a) corresponds to 0-th order multipole, and the interactions in Figure 2(b) can be viewed as (1/2)-th order multipole. (It is equivalent to (1/2)-th order multipole because of the amount of information computed. If we go down two levels, then it will be comparable to 1st order multipole.) The concept can be applied recursively for A_1 and A_2 respectively. As a result, panels high in the hierarchy tend to pass the interaction down more often than panels low in the hierarchy, and panels contain non-uniform charge tend to pass the interaction down more often than panels contain uniform charge distribution.

B. Application

Compared with the traditional FMM algorithms [12, 15] that improves the accuracy by increasing the expansion order for all nodes, our new scheme selects some nodes for high order expansion and leaves other nodes with ordinary expansion order. For nodes with large unbalanced charge distribution and large potential coefficient, i.e., large $\left| \left(q^t_{l_{left}} - q^t_{l_{right}} \right) \cdot p^t_{kl} \right|$, we use high order expansion.

Variable Order Multipole Scheme
Input: Conductors and threshold θ.
Output: Capacitance matrix $\mathbf{C}$.

1: Build low order multipole structure $\mathbf{P}^1$.
2: For each conductor i
3: $\quad t \leftarrow 1$.
4: $\quad$ Repeat
5: $\quad\quad$ Run GMRES to solve $\mathbf{P}^t \cdot \mathbf{q} = \mathbf{v}$ for one iteration, and let the result be $\mathbf{q}^t$.
6: $\quad\quad$ For each multipole coefficient p^t_{kl}, if $\left(\left| \left(q^t_{l_{left}} - q^t_{l_{right}} \right) \cdot p^t_{kl} \right| > \theta \right)$ then use high order expansion for p^{t+1}_{kl}, else use p^t_{kl} for p^{t+1}_{kl}.
7: $\quad\quad t \leftarrow t + 1$.
8: $\quad$ Until GMRES converges.
9: $\quad$ Compute the i-th row of $\mathbf{C}$ from $\mathbf{q}^t$.

Threshold θ is a user defined value that decides which coefficients are selected for high order expansion. In our implementation, high order expansion means going down the hierarchy as shown in Figure 2. Note that in step 6, we also rely on the fact that our algorithm stores the potential coefficients matrix in a data structure of size $O(n)$ [15]. Therefore step 6 takes only $O(n)$ time.

Experimental result is shown in Figure 4. The implemented algorithm is executed on a SUN UltraSPARC for the 4×4 conductor example used in [12] and [15]. The error of capacitance matrix $\bar{\mathbf{C}}$ is defined as $\|\bar{\mathbf{C}} - \mathbf{C}\|/\|\mathbf{C}\|$, where norm $\|\cdot\|$ is the Frobenius norm, and $\mathbf{C}$ is the accu-

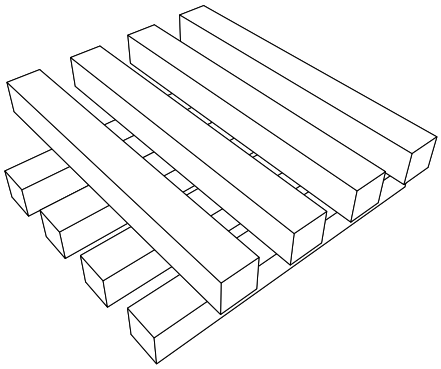

Fig. 3. The 4x4 conductor example.

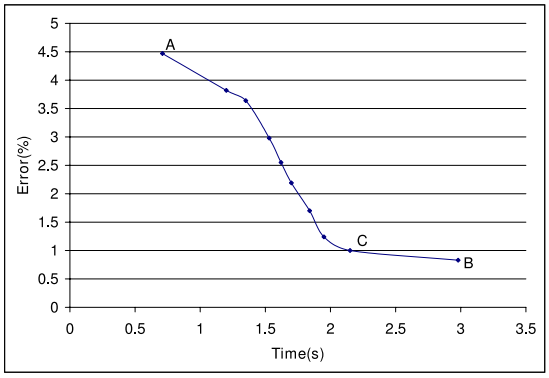

Fig. 4. Experimental result for variable order multipole scheme.

rate capacitance matrix computed by using direct method without FMM. Our GMRES reduces the two-norm residual to 1% from the initial residual.

In Figure 4, point **A** is for the case where all nodes have ordinary expansion order and point **B** is for the case where all nodes have high expansion order. Both **A** and **B** are based on the traditional hierarchical method. Points between **A** and **B** are from variable order multipole method with various θ.

From the curve in Figure 4, we find point **C** has comparable accuracy as **B** while uses much less time. This shows the advantage of the proposed scheme over traditional methods.

IV. Multigrid Scheme

It is obvious that if we use fine discretization, then the solution accuracy will be high, but the dimension of the linear system will be large. Therefore the time cost for solving fine discretization systems is also high. One way to reduce the time cost is to find a good initial solution to reduce the number of iterations.

The multigrid method is a fast linear iterative solver based on the multilevel or multi-scale paradigm [4]. The multigrid method uses several levels of refinement. The solution of each level is mapped to the next (finer) level and used as the initial value for solving the next (finer) level. Compared with the traditional method, the multigrid method may use the same number of iterations. However most systems solved by the multigrid method are small, thereby saving the total time. The multigrid method can be applied in combination with any of the common discretization techniques. In this section, we apply multigrid method to capacitance extraction.

Multigrid Scheme
Input: Conductors, convergence criteria ϵ_{coarse} and ϵ_{fine}.
Output: Capacitance matrix $\mathbf{C}$.

1: Discretize conductor surfaces coarsely and build corresponding coarse level linear system $\mathbf{P_{coarse}} \cdot \mathbf{q_{coarse}} = \mathbf{v_{coarse}}$.
2: Further discretize conductor surfaces and build corresponding fine level linear system $\mathbf{P_{fine}} \cdot \mathbf{q_{fine}} = \mathbf{v_{fine}}$.
3: For each conductor i,
4: Solve coarse level linear system for ${\mathbf{q_{coarse}}}^{(i)}$ with convergence criteria ϵ_{coarse}.
5: Map ${\mathbf{q_{coarse}}}^{(i)}$ to fine discretization ${\mathbf{q^0_{fine}}}^{(i)}$.
6: Solve fine level linear system for ${\mathbf{q_{fine}}}^{(i)}$ using ${\mathbf{q^0_{fine}}}^{(i)}$ as the initial value, with convergence criteria ϵ_{fine}.
7: Compute i-th row of matrix $\mathbf{C}$ using ${\mathbf{q_{fine}}}^{(i)}$.

In this algorithm, charges on each coarse panel are evenly mapped to its fine panels. Different convergence criteria ϵ_{coarse} and ϵ_{fine} are used for coarse level and fine level respectively. Usually, small ϵ_{fine} is chosen to guarantee the accuracy of the final solution. On the other hand, large ϵ_{coarse} is chosen because it provides sufficiently good initial solution at low computation cost.

Figure 5 is a comparison of multigrid method and traditional method for the 4×4 conductor example. For the traditional method, the conductors are divided into 17408 panels and the large system is solved directly with the convergence criteria $\epsilon = 0.01$. It takes 16 iterations to reduce the residual to less than 0.01. The computation time is 34.84 sec. For the multigrid method, the conductors are divided into 576 panels at the coarse level and further divided into 17408 panels at the fine level. With convergence criteria $\epsilon_{coarse} = 0.1$ and $\epsilon_{fine} = 0.01$, the number of iterations for coarse level and fine level are 5 and 11, respectively. Compared with the traditional method, multigrid method saves 5 iterations of solving a large system at the expense of 5 iterations of solving a small system. The total computation time is 26.72 sec, which is 23.2% less than that of the traditional method.

Our experience tells us that using more than two levels

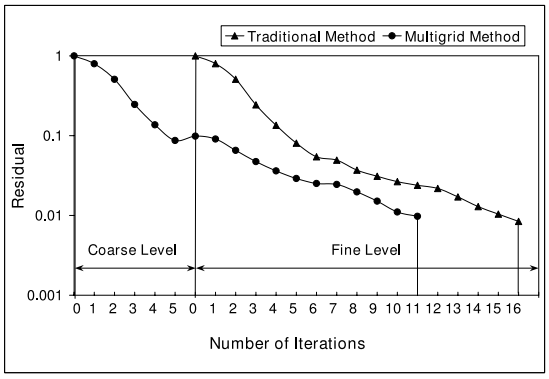

Fig. 5. Experimental result for multigrid scheme.

of refinement does not provide additional benefit. This is because for capacitance extraction, the total number of iterations is small. Therefore if there are three or more linear systems, then the number of iterations for the finest level will not decrease, while the overhead for setting up linear systems will increase.

V. Conclusion

We study three types of errors involved in the BEM for parasitic extraction. Using the sensitivity analysis for linear systems, we present a theory that clarifies the relationship between the error of each entry of the capacitance matrix and the error of the potential coefficients. Experiments based on this theory show that the accuracy for selected entries of the capacitance matrix can be improved greatly with a small increase in the overall computation time. We also propose a variable order multipole method that selects nodes with large unbalanced charge distribution for high order expansion, while keeps the expansion order of other nodes unchanged. The experiments show that the variable order multipole method is effective and practical in improving the overall accuracy of the capacitance matrix. Finally, we apply multigrid method for the first time to parasitic extraction. The experiments show the potential of the multigrid method. For inductance extraction where the number of iterations is usually large, the multigrid method may be more effective.

Acknowledgements

We authors thank Vivek Sarin and Xuan Zeng for discussions and suggestions.

References

[1] M. Bachtold, M. Emmenegger, J. G. Korvink, and H. Baltes, "An error indicator and automatic adaptive meshing for electrostatic boundary element simulations", *IEEE Trasn. CAD*, Vol. 16, No. 12, December 1997, 1439–1446.

[2] J. Barnes and P. Hut. "A hierarchical $O(n \log n)$ force calculation algorithm," *Nature*, Vol. 324, 1986.

[3] M. Beattie and L. Pileggi, "Electromagnetic parasitic extraction via a multipole method with hierarchical refinement," *Proc. 1999 ICCAD*, 437–444.

[4] W. L. Briggs, V. E. Henson, and S. McCormick, *A Multigrid Tutorial*, Second Edition, SIAM, Philadelphia, 2000.

[5] K. C. Donepudi, J. Song, J.-M. Jin, G. Kang and W. C. Chew, "A novel implementation of multilevel fast multipole algorithm for higher order Galerkin's method," *IEEE Trans. AP*, Vol. 48, No. 8, Aug. 2000, 1192–1197.

[6] G. H. Golub and C. F. Van Loan, *Matrix Computations*, 2nd ed., Johns Hopkins University Press, 1989.

[7] A. Grama, V. Sarin, and A. H. Sameh, "Improving error bounds for multipole-based treecodes," *SIAM J. Sci. Comput.*, Vol. 21, No. 5, 2000, 1790–1803.

[8] L. Greengard, *The Rapid Evaluation of Potential Fields in Particle Systems,* MIT Press, Cambridge, MA, 1988.

[9] M. Kamon, M. J. Tsuk and J. White, "FastHenry: A multipole-accelerated 3-D inductance extraction program," *IEEE Trans. MTT*, Vol. 42, No. 9, Sept. 1994, 1750–1758.

[10] S. Kapur and D. E. Long, "IES^3: A fast integral equation solver for efficient 3-dimensional extraction," *Proc. 1997 ICCAD*, 448–455.

[11] H. Mahawar, V. Sarin, and W. Shi, "A solenoidal basis method for efficient inductance extraction", *Proc. 2002 DAC*, 751–756.

[12] K. Nabors and J. White, "FastCap: A multipole accelerated 3-D capacitance extraction program," *IEEE Trans. CAD*, Vol. 10, No. 11, Nov. 1991, 1447–1459.

[13] J. R. Phillips and J. White, "A precorrected FFT method for capacitance extraction of complicated 3-D structures," *IEEE Trans. CAD,* Vol. 16, No. 10, Oct. 1997, 1059–1072.

[14] Y. Saad and M. H. Schultz, "GMRES: A generalized minimal residual algorithm for solving nonsymmetric linear systems," *SIAM J. Sci. Stat. Comput.*, Vol. 7, No. 3, July 1986, 856–869.

[15] W. Shi, J. Liu, N. Kakani and T. Yu, "A fast hierarchical algorithm for 3-D capacitance extraction", *IEEE Trans. CAD*, Vol. 21, No. 3, March 2002, 330–336.

[16] J. Tausch and J. White, "A multiscale method for fast capacitance extraction", *Proc. 1999 DAC*, 537–542.

[17] J. Tausch and J. White, "Mesh refinement strategies for capacitance extraction based on residual errors", *IEEE 5th Tropical Meeting*, 1996, 236–237.